CORROSION OF 316L STAINLESS STEEL ALLOY AND HASTELLOY-N SUPERALLOY IN MOLTEN EUTECTIC LiF-NaF-KF SALT AND INTERACTION WITH GRAPHITE

MATERIALS FOR NUCLEAR SYSTEMS

KEYWORDS: *molten salt, corrosion, graphite*

ROBERT S. SELLERS,[a] WEI-JEN CHENG,[a,b] BRIAN C. KELLEHER,[a] MARK H. ANDERSON,[a] KUMAR SRIDHARAN,[a]* CHAUR-JENG WANG,[b] and TODD R. ALLEN[a]

[a]*University of Wisconsin–Madison, Department of Engineering Physics, 1500 Engineering Drive Madison, Wisconsin 53711*
[b]*National Taiwan University of Science and Technology, Department of Mechanical Engineering Taipei 10607, Taiwan*

Received June 14, 2013
Accepted for Publication February 12, 2014
http://dx.doi.org/10.13182/NT13-95

Molten FLiNaK salt [46.5%LiF-11.5%NaF-42%KF (mol%)] has been proposed for use as a secondary reactor coolant and medium for transfer of high-temperature process heat from nuclear reactors to chemical plants. Two alloys—Hastelloy-N superalloy (Hastelloy-N) and Type 316L stainless steel alloy (316L steel)—were exposed to molten FLiNaK salt in a 316L steel crucible under argon cover gas at 850°C for 1000 h. Graphite was also introduced into the test with the goal of studying the corrosion behavior of relevant reactor material combinations. The results show that corrosion of 316L steel occurred primarily through surface depletion of Cr. Contrarily, Hastelloy-N experienced weight gain due to the electrochemical plating of corrosion products, Fe and Cr, derived from the 316L steel crucible. The graphite sample enhanced the corrosion of the 316L steel sample and crucible, which induced the formation of $(Cr,Fe)_7C_3$ and $(Mo,Cr,Fe)_2C$ carbides on the surface of graphite. These carbide formations were attributed to the nonelectric transfer between 316L steel and graphite. Besides reducing the availability of chromium to plate, the presence of graphite did not change the basic corrosion of the 316L steel and plating process of Hastelloy-N.

Note: Some figures in this paper may be in color only in the electronic version.

I. INTRODUCTION

Generation IV nuclear initiatives have selected molten fluoride salts as potential reactor coolants for the transfer of high-temperature process heat for hydrogen and other chemical production plants.[1] The eutectic fluoride salt mixture 46.5%LiF-11.5%NaF-42%KF (mol%), commonly referred to as FLiNaK, is emerging as a leading candidate for use as a secondary heat transfer fluid due to its advantageous thermophysical properties compared to water or pressurized helium, characterized by high thermal conductivity, high specific heat, low viscosity, and high boiling point (Table I). However, at the high temperatures required for a chemical processing plant, material corrosion presents an engineering challenge because of the reduction-oxidation (redox) reaction of fluorine ions with surface protective oxide

*E-mail: kumar@engr.wisc.edu

TABLE I

Comparison of Thermophysical Properties of Molten FLiNaK Salt and Water

Fluid	T_m (°C)	ρ (g/cm^3)	ρ·Cp (cal/cm^3·°C)	μ (cP)	k (W/m·K)	Boiling Point at 1 atm (°C)
FLiNaK at 700°C	454	2.02	0.91	2.9	0.92	1570
H_2O at 20°C	0	1	0.44	1	0.6	100

scales of Cr, Al, or Si. In molten fluoride salts, these oxide scales are chemically unstable. Thus, the passivating properties typically exhibited by heat-resistant alloys are rendered ineffective.

The corrosion characteristics of a variety of materials in contact with molten FLiNaK salt have been studied.[2–5] It has been shown that the common structural alloying elements used in Fe- and Ni-based alloys have a propensity to be corroded in molten fluoride salts in the following order: Ni, Co, Fe, and Cr, with Cr being the most prone to dissolution because of its least negative Gibbs free energy of fluoride formation.[2,3] The dissolution of Cr renders the corrosion-resistant passivating scale, Cr_2O_3, on alloys ineffective. It has been observed in past molten fluoride static tests that the corrosion rate of different alloys correlates to the percent Cr composition, in which the corrosion rate of alloys increased as the Cr content increased.[2]

Two alloys—Type 316L stainless steel alloy (316L steel) and Hastelloy-N superalloy (Hastelloy-N)—were exposed to molten FLiNaK salt in this study. 316L steel is a common low-carbon Fe-Ni-Cr–based alloy with widespread industry use. 316L steel has the advantage of *ASME Boiler and Pressure Vessel* Code, Sec. III (BPVC-III) high-temperature certification and exhibits adequate long-term creep rupture strength at elevated temperatures.[6] Hastelloy-N is a Ni-Mo-Cr–based superalloy developed by Oak Ridge National Laboratory (ORNL) during the Aircraft Reactor Experiment and used as a structural alloy during the Molten Salt Reactor Experiment (MSRE) specifically as a fluoride salt corrosion-resistant material.[7,8] The nominal elemental compositions for 316L steel and Hastelloy-N are included in Table II. Corrosion studies were a strong focus of ORNL scientists in the MSRE era when access to Hastelloy-N was abundant. The variety and depth of these studies do an excellent job of establishing the baseline corrosion characteristics for some experimental conditions like static isothermal and convection loops in several molten salt mixtures. Experiments performed in the 1960s and 1970s demonstrate a low rate of corrosion in the form of weight loss for Hastelloy-N in certain conditions.[9,10] However, previous testing during the MSRE was performed at lower temperatures (650°C), so corrosion resistance has not been established at the elevated temperatures required by a chemical production plant.[11]

In addition, proposed designs for next-generation reactors have specified BPVC-III alloys clad in Hastelloy-N as potential vessel and structure construction material in order to have a solution for corrosion and BPVC-III restrictions. Unless Hastelloy-N is to be BPVC-III certified, is it pertinent to study the immersion of material combinations in molten salts until more sophisticated experiments can be developed to study delamination events in corrosive molten salt environments.[12,13]

Previous static corrosion tests in molten FLiNaK salt have focused primarily on exposing a wide range of alloys to the same molten salt environment or modifying the redox environment of the molten salt.[2,14] The focus of this study is to expose two candidate alloys—316L steel and Hastelloy-N—to molten FLiNaK salt at 850°C for 1000 h in a 316L steel crucible. This is done in order to imitate material interactions in a practical advanced nuclear reactor environment. Additionally, Olson et al.[2] and Ozeryanaya[15] have shown that the presence of graphite can aid in the corrosion of some alloys through a nonelectric transfer effect. As some Generation IV reactor

TABLE II

Nominal Chemical Compositions for 316L Steel and Hastelloy-N*

Element	C	Fe	Ni	Mn	Si	Cr	Mo	P	S
316L steel	0.02	[a]	10.27	1.64	0.52	17.23	2.22	0.03	0.02
Hastelloy-N	0.08[b]	4.12	[a]	0.66	0.76	7.30	16.19	—	—

*In units of weight percent.
[a]As balance.
[b]Maximum.

designs contain large quantities of graphite,[16] effort was also made to observe the graphite-alloy interaction in the molten FLiNaK salt environment.

II. EXPERIMENTAL

The FLiNaK used for this static test was produced in University of Wisconsin–Madison (UW-Madison) facilities. Source components were procured from Alfa-Aesar and Noah Technologies. The components were combined in the correct ratios under an anhydrous argon atmosphere glove box and slowly brought up to high temperature (700°C) in a silicon carbide (SiC) crucible to form a homogeneous melt. Figure 1 shows the test system for the five crucibles. All crucible components are made of 316L steel. All components were machined to remove manufacturing scale and surface impurities. Following machining, all crucible materials were cleaned with phosphoric acid and other solvents to remove residual oil and grime left over from fabrication. 316L steel coupons were laser cut to size from 18 gauge sheet. Hastelloy-N coupons were taken from existing stock. All coupons were drilled with diagonally opposing holes for mounting and underwent a polishing process with SiC paper to 1200-grit finish. Following polishing, they were engraved and ultrasonically cleaned in ethanol and deionized water. Last, the coupons were dried and weighed on a high-accuracy microgram scale.

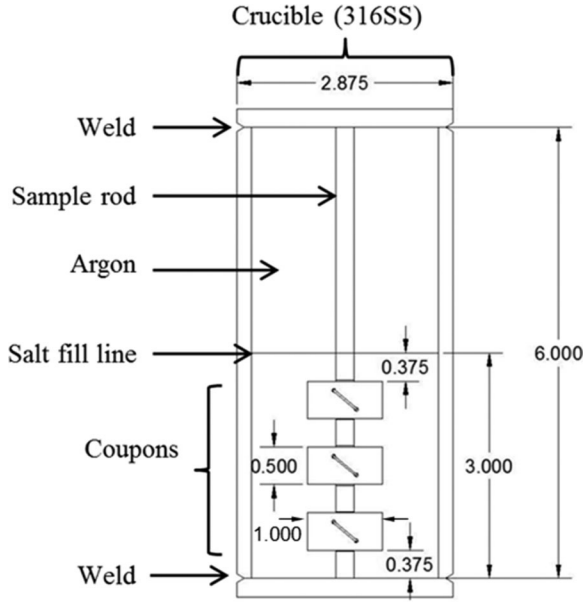

Fig. 1. Schematic view of the static corrosion test crucible. All crucible materials are made of 316L steel. All measurements are in inches. The coupons are attached to the sample rod by 316L steel wire.

Three of the crucibles contained two metallic coupons and one graphite coupon located in the middle slot of the coupon stand. The purified graphite was procured from POCO, grade AFX-5Q with an average particle size of 5 μm and average pore size of 0.8 μm (Ref. 17). The surface area of each alloy coupon and alloy vessel were 6.5 and 237 cm^2, respectively. The graphite was milled to have approximately twice the surface area of a single metallic coupon. Following milling, the graphite was labeled, ultrasonically cleaned in ethanol and deionized water, dried, and weighed. Once all coupons and graphite pieces were tied to the sample rods in the correct order via cleaned 316L steel wire, they were placed in the glove box to join the salt and other crucible materials. Previous tests relied on a hot active transfer system where salt was moved in liquid form from a heated container to a heated crucible,[2] but it was determined that using a cold technique would be suitable and allow for greater control over the quantity of salt placed in the crucible. The final steps included the addition of 513 +/− 2.5 g of pulverized salt to each crucible followed by a finishing weld to close the crucible. All finishing steps were performed in an argon atmosphere glove box.

During the corrosion process, the furnace was ramped to 850°C at a rate of 200°C/h and then held at 850°C for 1000 h in inert nitrogen atmosphere. For safety reasons, the furnace temperature was lowered to 550°C at the conclusion of the 1000 h so the crucibles could be removed individually and turned upside down to cool. This caused the salt to solidify while not in contact with the coupons, making the sample rod removal easier. The crucible tops were removed with an abrasive disk handsaw. Sample rods were pulled from the salt bed and cleaned ultrasonically in 1 *M* $Al(NO_3)_3$ solution to speed the dissolution of the FLiNaK salt. During the material preparation stage and throughout the corrosion test, effort was made to abide by guidelines laid out by ASTM International[18] and NACE International[19] such as abiding by suggested sample cleaning procedures, standards of furnace temperature regulation, and recommended polishing practices. The corrosion levels of the samples were evaluated using weight change measurement. Characterization of the top-view and cross-sectional morphologies of the samples was carried out by scanning electron microscopy (SEM) with energy dispersive spectrometry (EDS), X-ray diffraction (XRD), and electron backscatter diffraction (EBSD).

III. RESULTS AND DISCUSSION

III.A. Weight Change of 316L Steel and Hastelloy-N

The results of weight changes of 316L steel and Hastelloy-N samples after FLiNaK exposure at 850°C for 1000 h are shown in Fig. 2. All 316L steel samples lost

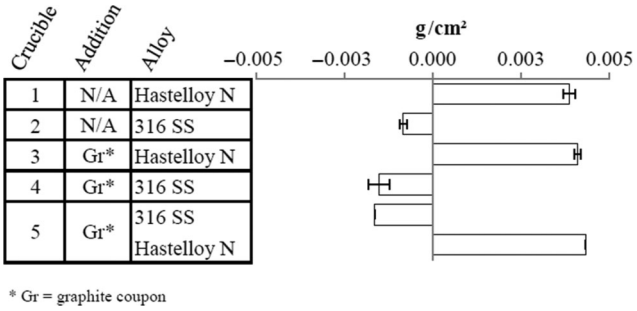

Fig. 2. Weight change of all crucible scenarios after corrosion testing performed in a 316L steel crucible filled with FLiNaK at 850°C for 1000 h. Error bars designate weight change standard deviation of the sample set.

weight during the static corrosion test while all of the Hastelloy-N samples gained weight. The presence of graphite causes an increase in weight loss for 316L steel, while the presence of graphite appears to have no significant effect on the weight change of Hastelloy-N. In a previous study[2] of materials corrosion in graphite crucibles after FLiNaK exposure at 850°C for 500 h, it has been shown that all of the iron-based and nickel-based high-temperature alloys lost weight.

Although 316L steel was not exposed to FLiNaK in the previous study, it is useful to compare the weight loss measured by Olson et al. of Hastelloy-N ($\sim$3 mg/cm^2 loss) and Incoloy-800H ($\sim$30 mg/cm^2 loss) exposed to FLiNaK in a graphite crucible[2] against the 316L steel weight loss results of this test ($<$3 mg/cm^2 when in contact with graphite). Conventional wisdom dictates that higher Ni-containing alloys should experience less attack; however, it can be seen that the higher Ni-containing alloys exposed to FLiNaK by Olson et al. lost more weight than the 316L steel samples exposed in this test. Additionally, the exposure time of this test is twice that of the previous test performed by by Olson et al. A possible explanation for the disparity is that the area ratio of graphite to sample in the previous study by Olson et al. is approximately 170 times larger than the area ratio of graphite to sample in this study. This suggests the area ratio of graphite to sample has a strong effect on the extent of material corrosion, in which the corrosion rate of materials would be accelerated by a larger area ratio of graphite to sample. On the other hand, the weight gain behavior of Hastelloy-N in this test is contradictory to the normal behavior of materials exposed in static molten FLiNaK, implying that material can deposit on Hastelloy-N using molten salt as a transport medium.

III.B. 316L Steel

Figure 3 contains the plan-view and cross-sectional SEM micrographs with the corresponding EDS line-scan analysis of 316L steel samples. The EDS element line scan from the inner 316L steel substrate to its surface shows that Fe increases and Cr decreases relatively, while Ni and Mo have no change. Also, XRD analysis reveals that the surface of 316L steel after corrosion is γ-austenite, which is the same as 316L steel. These results imply that 316L steel experienced typical Cr dissolution behavior. Corrosion of 316L steel is more severe when graphite is present in the system, which is evident through greater measured weight loss and surface Cr depletion depth. The approximate depths of Cr depletion for 316L steel and 316L steel with graphite are 40 and 50 μm, respectively. Some voids can also be observed at the grain boundaries in the outer substrate. The formation of these voids is associated with precipitates in 316L steel at grain boundaries formed during the high-temperature, long-duration corrosion test, which acted as an annealing process. EDS analysis reveals the composition of these precipitates to be 57Fe-33Cr-4Ni-6Mo (at. %), identified as σ-$(Fe,Ni)_3(Cr,Mo)_2$. The formation of σ-$(Fe,Ni)_3(Cr,Mo)_2$ has been observed in 316L steel held at 650°C to 900°C for long periods of time.[20] This elevated Cr content of σ-$(Fe,Ni)_3(Cr,Mo)_2$ over the nominal 18 at. % Cr of the 316L steel matrix caused σ-$(Fe,Ni)_3(Cr,Mo)_2$ to be preferentially corroded, leading to the void formations. The observation that the size of voids in 316L steel with graphite present is larger than that in 316L steel without graphite present also proves the corrosion acceleration effect of 316L steel by graphite.

Figure 4 shows the change in visual characteristics of graphite samples tested with 316L steel. The graphite sample was covered with a silver coating, containing major Cr and minor Fe (Cr:Fe at. % ratio is $\sim$10) exposed by EDS analysis. XRD identified the coating on graphite, which was found to match Cr_7C_3 carbide as shown in Fig. 5. Because the minor Fe were detected in the coating on graphite, the Cr_7C_3 revealed by XRD should be modified as $(Cr,Fe)_7C_3$, in which Fe entered into solid solution in Cr_7C_3. A cross-sectional SEM micrograph of graphite samples (Fig. 6a) shows surface $(Cr,Fe)_7C_3$ formation $\sim$10 μm thick. Additionally, some bright particles could be found in $(Cr,Fe)_7C_3$. EDS revealed these bright particles to be rich in Mo and Cr, as well as a few atomic percent Fe particles (Mo:Cr:Fe at. % ratio is 7:3:1). Phase identification of the bright particles was carried out by EBSD due to the inability of EDS to provide accurate carbon measurement. An EBSD phase distribution map of the $(Cr,Fe)_7C_3$ coating containing bright particles revealed that the bright particles are Mo_2C carbide as shown in Fig. 6b. According to the EDS observation of the presence of Cr and Fe in Mo_2C carbide, Cr and Fe are considered to stay as solid solution form in Mo_2C. Thus, Mo_2C should be modified as $(Mo,Cr,Fe)_2C$.

Our previous molten FLiNaK static corrosion tests performed in graphite crucibles indicated the formation of $(Cr,Fe)_7C_3$ on graphite.[2] The $(Cr,Fe)_7C_3$ plating process occurs through the nonelectric transfer of Cr and Fe from

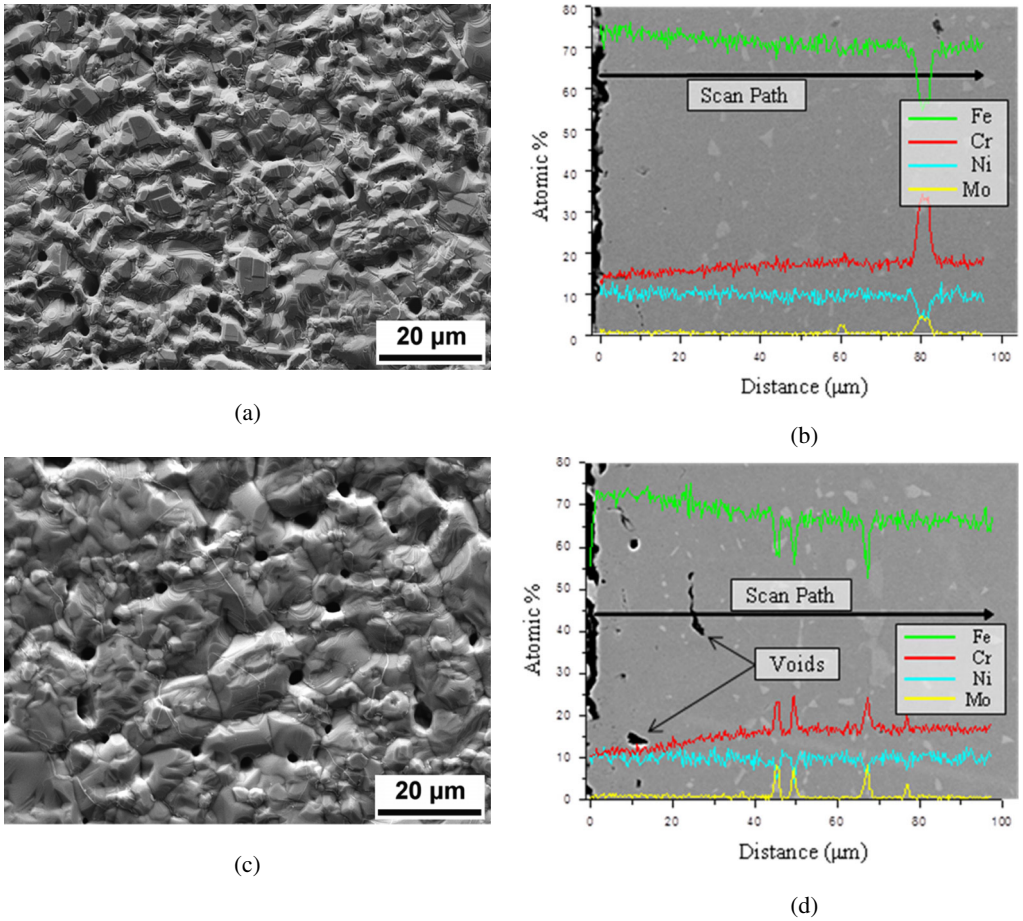

Fig. 3. Top-view and cross-sectional SEM micrographs and corresponding EDS line-scan analysis of 316L steel samples tested (a) and (b) without graphite, and (c) and (d) with graphite, in FLiNaK at 850°C for 1000 h.

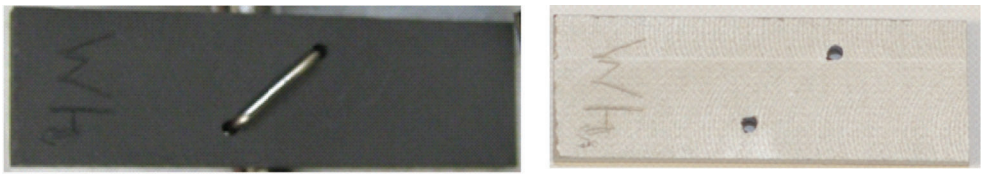

Fig. 4. (a) Typical graphite coupon appearance prior to exposure to FLiNaK at 850°C for 1000 h. (b) Graphite coupon after cleaning showing the presence of the chrome carbide coating. The length is shorter because a cross section of the sample has been taken.

316L steel to electropositive graphite as described by Ozeryanaya.[15] This nonelectric effect accelerated the dissolution of Cr and Fe contained in 316L steel when graphite is present, which had been reflected in its weight change result. The formation of small amounts of $(Mo,Cr,Fe)_2C$ on graphite implies that Mo in the 316L steel sample and crucible would still be corroded by FLiNaK; however, based on the fluoride formation free energy, Mo is nobler than Cr, Fe, and Ni in FLiNaK. Since Ni was not detected in the graphite coating and the fluoride formation free energy of Ni is more negative than Mo, the formation of $(Mo,Cr,Fe)_2C$ can be attributed to the same mechanism as $(Cr,Fe)_7C_3$, i.e., the nonelectric transfer of Mo from 316L steel to graphite.

III.C. Hastelloy-N

Contrary to the corrosion behavior of the 316L steel coupons in this study as well as existing Hastelloy-N corrosion studies, all Hastelloy-N samples gained weight

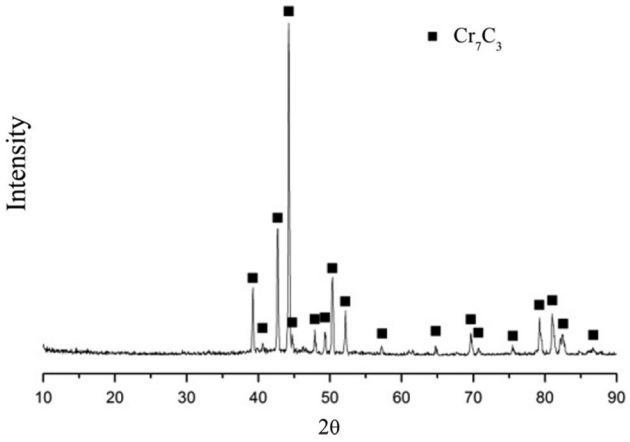

Fig. 5. XRD analysis of graphite coupon tested with 316L steel in FLiNaK at 850°C for 1000 h.

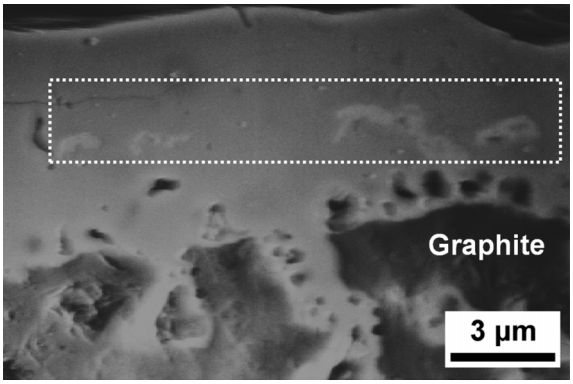

(a)

(b)

Fig. 6. (a) Cross-sectional SEM micrograph of graphite coupon tested with 316L steel in FLiNaK at 850°C for 1000 h. (b) EBSD phase distribution map of the white dotted rectangular area on SEM micrograph. Green and red phases represent Cr_7C_3 and Mo_2C, respectively. Coating on graphite sample was composed of major Cr_7C_3 and minor Mo_2C particles.

while exposed to FLiNaK in the 316L steel crucible at 850°C for 1000 h. Top-view SEM micrographs of Hastelloy-N without graphite present display the morphology of polyhedral-shaped grains on the surface, which indicated that Hastelloy-N underwent a diffusion process as shown in Fig. 7a. Figure 7b shows the cross-sectional SEM micrographs and corresponding EDS line-scan analysis of Hastelloy-N samples not in contact with graphite. From the inner substrate to the sample surface, the Fe and Cr line-scan profiles increased while the Ni and Mo line-scan profiles decreased, suggesting Ni/Mo dissolution. However, this conclusion is contrary to the nature of material corrosion in FLiNaK, in which Ni and Mo are more passive than Fe and Cr.

Although the XRD analysis shows that the crystal structure of the sample surface is γ-austenite, which is the same as Hastelloy-N, the weight gain of Hastelloy-N and the formation of the Fe- and Cr-rich outer layer give strong evidence of an Fe/Cr deposit process instead of Ni/Mo dissolution. A similar result has been described by Kondo et al.[4,5] Because of the large Ni content of Hastelloy-N, it is believed that the coupons acted as a cathode whereby corrosion products (Fe and Cr) dissolved from the 316L steel crucible plated to the surface of Hastelloy-N. This deposit process is explained through the position of Ni on electromotive potential (EMP) series in molten FLiNaK salt as shown in Table III. Nickel is more electropositive than Fe and Cr and thus acts as a cathode. Once Fe and Cr deposited on the Hastelloy-N surface, it caused the inward diffusion of Fe and Cr and outward diffusion of Ni and Mo. The top-view and cross-sectional SEM micrographs and corresponding EDS line-scan analysis (Figs. 7c and 7d) reveal that Hastelloy-N with the presence of graphite underwent the same Fe and Cr deposit process as Hastelloy-N without the presence of graphite. However, the presence of graphite influenced the composition of the deposit layer to contain more Fe and less Cr, resulting in larger substrate Ni diffusion. The reason for this is the deposit formation on the graphite surface caused by the nonelectric transfer effect between the graphite and 316L steel crucible.

The graphite deposit has the same microstructure as observed on the graphite tested with 316L steel samples: major $(Cr,Fe)_7C_3$ with a small number of $(Mo,Cr,Fe)_2C$ particles. Thus, graphite can be seen as a Cr sink causing a decrease in the amount of Cr available to plate to the surface of the Hastelloy-N sample, resulting in the proportional increase of Fe in the deposit on Hastelloy-N. Since more Fe deposited on the Hastelloy-N, more Ni from the substrate could diffuse outward. On the other hand, the formation of $(Mo,Cr,Fe)_2C$ has proved that graphite causes Mo dissolution of the 316L steel crucible. The same mechanism for Mo dissolution should also happen to the Hastelloy-N sample because it has a larger Mo content (~16 wt%). However, the deposit of Fe and Cr covered the Hastelloy-N sample and impeded the exposure of the sample to FLiNaK. The speculation of Mo dissolution from Hastelloy-N warrants further investigation. It is worth emphasizing the contradictory weight-gain behavior of Hastelloy-N in this study compared with Hastelloy-N of previous ORNL experiments. Because of the electroplating, this experiment precludes direct comparison with previous studies because the true Hastelloy-N surface is shrouded in corrosion product.

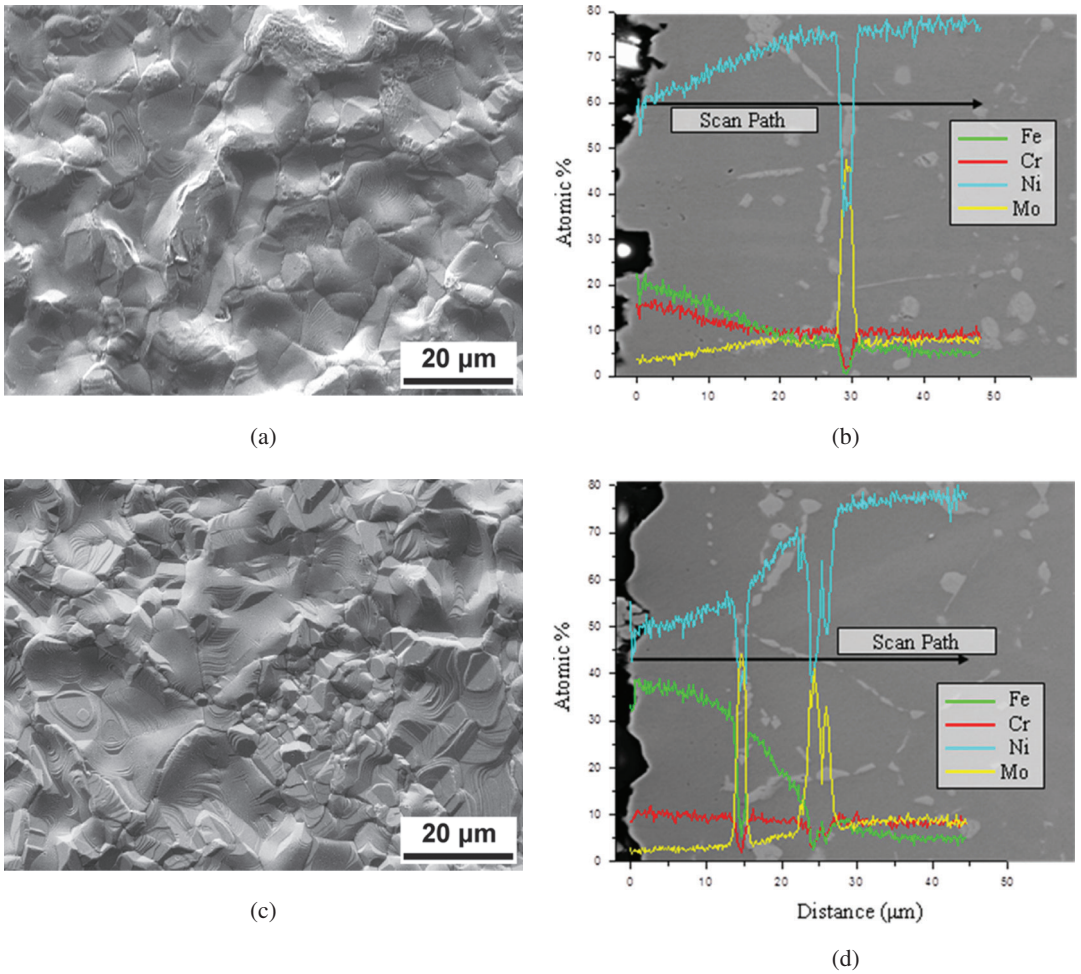

Fig. 7. Top-view and cross-sectional SEM micrographs and corresponding EDS line-scan analysis of Hastelloy-N samples tested (a) and (b) without graphite, and (c) and (d) with graphite, in FLiNaK at 850°C for 1000 h.

TABLE III

EMP Series for Transition Metal Ions in Molten FLiNaK at 750°C in Reference to the Standard Potential of a Ni^{2+}/Ni Couple That Was Set to Zero

Half-Cell Reaction	Standard Potential (Volts Versus Standard Ni^{2+}/Ni Electrode)
$Ni^{2+} + 2e^- = Ni$	0
$Fe^{3+} + 3e^- = Fe$	−0.21
$Fe^{2+} + 2e^- = Fe$	−0.512
$Cr^{2+} + 2e^- = Cr$	−0.69
$Cr^{3+} + 3e^- = Cr$	−1.13
$Zr^{4+} + 4e^- = Zr$	−1.25

III.D. Alloy Interaction in a Reactor Environment

The tendency for the more noble nickel-based Hastelloy-N to act as a sink for corrosion products derived from 316L steel could have implications for any next-generation reactor design incorporating a BPVC-III alloy clad in Hastelloy-N. The two most popular options for BPVC-III alloys, 800H and 316 grade stainless, both have compositions different from the rather unique Ni-Mo-Cr composition of Hastelloy-N and could be expected to act as the anode in a system containing the more noble Hastelloy-N, with the rate and transport quantity depending on relative alloy surface areas. Should a Hastelloy-N–clad reactor experience a small delamination or erosion event, it would expose the underlying structural metal to a vast cathode surface area. As a result, this delamination point could experience corrosion at a much quicker rate.

IV. CONCLUSION

The corrosion behavior of 316L steel and Hastelloy-N and their interaction with graphite in molten FLiNaK salt were studied using a static corrosion test in a 316L steel

crucible at 850°C for 1000 h. The 316L steel samples experienced weight loss that was accounted for by surface Cr depletion. When graphite was present in the system, 316L steel coupons have nearly double weight loss in addition to larger void formations near the surface. This accelerated corrosion of 316L steel was caused by the nonelectric transfer of Cr, Fe, and Mo from 316L steel to the graphite surface to form $(Cr,Fe)_7C_3$ and $(Mo,Cr,Fe)_2C$ carbides. Hastelloy-N coupons, on the other hand, form an Fe- and Cr-rich deposit layer on its surface. The formation of this deposit layer is due to an electrochemical plating process of 316L steel crucible corrosion products (Fe and Cr) on Hastelloy-N, followed by Fe and Cr inward diffusion and Ni and Mo outward diffusion. The nonelectric transfer between graphite and the 316L steel crucible influenced the plating behavior of Hastelloy-N by decreasing the amount of Cr available to plate to the surface, leading to a deposit composition with more Fe and less Cr than the Hastelloy-N system containing no graphite. Mo_2C carbide evolution on graphite may represent another attack mode on Hastelloy-N and warrants further investigation in a strict Hastelloy-N environment. Furthermore, if BPVC-III alloys clad in Hastelloy-N are to become mainstays of next-generation molten salt reactor designs, the consequences of cladding instability must be understood through more sophisticated corrosion studies.

ACKNOWLEDGMENTS

The authors are very grateful to the U.S. Department of Energy for funding support under grants DOE-FC07-05ID14675 and DOE-FC07-07ID14826. This research utilized National Science Foundation–supported shared facilities at UW-Madison.

REFERENCES

1. D. E. HOLCOMB and S. M. CETINER, "An Overview of Liquid-Fluoride-Salt Heat Transport Systems," ORNL/TM-2010/156, Oak Ridge National Laboratory (2010).

2. L. C. OLSON et al., "Materials Corrosion in Molten LiF-NaF-KF Salt," *J. Fluorine Chem.*, **130**, 67 (2009); http://dx.doi.org/10.1016/j.jfluchem.2008.05.008.

3. A. K. MISRA and J. D. WHITTENBERGER, "Fluoride Salts and Container Materials for Thermal Energy Storage Applications in the Temperature Range 973 to 1400 K," *Proc. 22nd Intersociety Energy Conversion Engineering Conf.*, Philadelphia, Pennsylvania, August 10–14, 1987, p. 10, American Institute of Aeronautics and Astronautics (1987).

4. M. KONDO et al., "Corrosion Characteristics of Reduced Activation Ferritic Steel, JLF-1 (8.92Cr–2W) in Molten Salts Flibe and Flinak," *Fusion Eng. Des.*, **84**, 1081 (2009); http://dx.doi.org/10.1016/j.fusengdes.2009.02.046.

5. M. KONDO et al., "Corrosion of Reduced Activation Ferritic Martensitic Steel JLF-1 in Purified Flinak at Static and Flowing Conditions," *Fusion Eng. Des.*, **85**, 1430 (2010); http://dx.doi.org/10.1016/j.fusengdes.2010.03.064.

6. *ASME Boiler and Pressure Vessel Code*, Sec. III, "Rules for Construction of Nuclear Facility Components," Division 1, Subsection NH, Class 1, "Components in Elevated Temperature Service," American Society of Mechanical Engineers (2007).

7. J. H. DEVAN, "Effect of Alloying Additions on Corrosion Behavior of Nickel-Molybdenum Alloys in Fused Fluoride Mixtures," ORNL/TM-2021, Oak Ridge National Laboratory (1969).

8. P. N. HAUBENREICH and J. R. ENGEL, "Experience with the Molten-Salt Reactor Experiment," *Nucl. Appl. Technol.*, **8**, 118 (1970); http://dx.doi.org/10.13182/NT70-1.

9. J. H. DEVAN and R. B. EVANS, "Corrosion Behavior of Reactor Materials in Fluoride Salt Mixtures," ORNL/TM-328, Oak Ridge National Laboratory (1962).

10. J. R. KEISER, "Compatibility Studies of Potential Molten-Salt Breeder Reactor Materials in Molten Fluoride Salts," ORNL/TM-5783, Oak Ridge National Laboratory (1977).

11. D. WILLIAMS, L. TOTH, and K. CLARNO, "Assessment of Candidate Molten Salt Coolants for the Advanced High-Temperature Reactor (AHTR)," ORNL/TM-2006/12, Oak Ridge National Laboratory (2006).

12. V. K. VARMA et al., "AHTR Mechanical, Structural, and Neutronic Preconceptual Design," ORNL/TM-2012/320, Oak Ridge National Laboratory (2012).

13. D. E. HOLCOMB et al., "An Analysis of Testing Requirements for Fluoride Salt-Cooled High Temperature Reactor Components," ORNL/TM-2009/297, Oak Ridge National Laboratory (2009).

14. W.-J. CHENG et al., "Zirconium Effect on the Corrosion Behavior of 316L Stainless Steel Alloy and Hastelloy-N Superalloy in Molten Fluoride Salt," *Nucl. Technol.*, **183**, 248 (2013); http://dx.doi.org/10.13182/NT12-125.

15. I. N. OZERYANAYA, "Corrosion of Metals by Molten Salts in Heat-Treatment Processes," *Metal Sci. Heat Treatment*, **3**, 184 (1985); http://dx.doi.org/10.1007/BF00699649.

16. "A Technology Roadmap for Generation IV Nuclear Energy Systems," GIF-002-00, U.S. Department of Energy (2002).

17. "AXF-5Q," POCO Incorporated (2012); http://www.poco.com/MaterialsandServices/Graphite/IndustrialGrades/AXF5Q.aspx (current as of Sep. 8, 2014).

18. "Standard Practice for Laboratory Immersion Corrosion Testing of Metals," G 31-72, ASTM International (2004).

19. "Standard Test Method—Laboratory Corrosion Testing of Metals," TM0169-2000, NACE International (2000).

20. B. WEISS and R. STICKLER, "Phase Instabilities During High Temperature Exposure of 316 Austenitic Stainless Steel," *Metall. Mater. Trans. B*, **3**, 851 (1972); http://dx.doi.org/10.1007/BF02647659.